Egyptian Journal of Chemistry
http://ejchem.journals.ekb.eg/

Characterization of Nano-crystalline Samaria-Fe and Yttria-Fe Co-doped Ceria Solid Solutions Prepared by Hydrothermal Technique

H.A. Badr, N. M. Ghoneim and A. El-Maghraby*
Department of Ceramics, National Research Center, Dokki, 12622, Cairo, Egypt.

POWDERS of Samaria, Yttria doped ceria and co-doped with iron were synthesized by hydrothermal method. The iron content for all the investigated compositions is 0.5 wt. %. The powders were investigated by thermogravimetric analysis (TGA) X-ray diffraction (XRD), Infrared (IR), Transmission electron microscope (TEM) and Raman spectra. The effect of autoclaving time on the crystallinity was studied. The powders were impacted and sintered at different temperatures. The density and linear shrinkage were investigated for all sintered bodies. XRD revealed that the powders crystallize in fluorite centered cubic structure with the improvement in crystallinity. The presence of iron in the solid solution lowered the degree of crystallinity. TEM images for the co-doped powders displayed semi-rounded nano-sized particles with narrow size distribution. It is concluded that the optimum fluorite structure for solid solutions is obtained with 10 mol % Samaria doped ceria (10SDC)Fe and iron codoped 10 mol % Yttria doped ceria (10YDC) Fe samples.

Keywords: Ceria, Co-doped, Hydrothermal, Samaria, Yttria, Transition metals.

Introduction

Ceria has been attracting a big deal of attention given its unique properties. Cerium oxide shows high ionic conductivity and therefore, is a hopeful material for applications of solid electrolytes in electrochemical devices such as fuel cells or catalytic reactors. A solid oxide fuel cell (SOFC) is an electrochemical device that turns the chemical fuels (such as methane, butane, hydrogen or gasoline and diesel) into electrical energy by the reaction of oxygen and hydrogen**.**

Solid oxide fuel cell (SOFC) is a simple device. The unit consists of four functional components: cathode, electrolyte, anode and interconnect. The solid electrolyte is a basic component of the SOFCs, and it must perform high ionic conductivity to facilitate the flow of oxygen ions [1]. Yttria Stabilized Zirconia (YSZ) is the most widely studied solid electrolyte ion conductor for SOFCs. However, cells with electrolytes of YSZ must operate at temperatures above 800 ºC to get satisfactory output, this high temperature leads to high costs of interconnect and construction materials. Also, it has problems with thermal degradation, thermal expansion and long term stability [2]. Doped ceria is another most promising high-conducting solid electrolyte for SOFCs and it can operate effectively at intermediate temperatures (600-700ºC).

In contrast to pure zirconia, $CeO_{2-\delta}$ has the fluorite structure together with oxygen vacancies ($V_o^{\cdot\cdot}$) as the predominant ionic defects [3 -7].

$$Ce_{Ce}^{x} + O_o^x \rightarrow 2e' + V_o^{\cdot\cdot} + 1/2\,O_2$$ Where:

(Ce^x_{Ce}) = Ce^{4+}, (Ce'_{ce}) = Ce^{3+} and (O_o^x) is O^{2-} ion on a regular O lattice site.

The oxygen vacancy concentration and the oxide ion conductivity in cerium oxide increased by the substitution of a lower-valiant metal ion for cerium by trivalent Sm^{3+}, Gd^{3+}, and Y^{3+} ions [3]. Recently, co-doped CeO_2 electrolytes attracted too much alertness to improve the electrical conductivity or the sintering properties. Co-

*Corresponding author e-mail: aelmaghraby60@hotmail.com
Received 19/9/2018; Accepted 13/11/2018
DOI: 10.21608/EJCHEM.2018.5187.1460
©2019 National Information and Documentation Center (NIDOC)

doping has advantages, such a decrease of defect association enthalpy, increase of configurationally entropy, and scavenging of impurity phases in grain boundaries. Therefore, co-doping ceria with alkaline earth and rare earth ions leads to higher conductivities than the single doped ceria [8]. Ceria has been doped with transition metal oxides to be used as electrolyte of solid oxide fuel cell. It is reported [9] that the small amounts of Fe_2O_3 strongly enhanced the densification rate with lower in sintering temperature and promoted the grain boundary mobility. To overcome the drawbacks of single doping, more recently mixed cations have been used to co-dope ceria ceramic electrolytes. Rare earth co-doping has been recently chosen to enhance the conductivity and the stability in doped ceria [10&11]. Gd_2O_3 and Sm_2O_3 are widely used as the dopants in the ceria ceramic electrolytes because the ionic size of Gd^{3+} and Sm^{3+} matches with the host Ce^{4+}. Babu and coworkers [12] processed Gadolinia (Gd_2O_3) doped ceria (GDC) and GDC co-doped with Eu_2O_3 (Eu-GDC) and Nd_2O_3 (Nd-GDC) in a one step by citrate-nitrate solution combustion reaction and impedance spectroscopy analysis was done to understand the conduction behavior. It was found that the grain boundary conductivity exhibited ionic character, which influenced by the space-charge layer and defect chemistry. The conductivity was improved in Nd- GDC while Eu-GDC showed similar conductivity as GDC [10]. The behavior of CGO ($Ce_{0.80}Gd_{0.20}O_{2-\delta}$) ceramics containing 2 mole % $CoO_{1.333}$ was Investigated [13]. They reached the following results; (a) a 2 % Co-CGO ceramics with 95-99 % density were achieved by firing at 1173-1373 ºK, and (b) bulk conductivity increases with increasing firing temperature [14]. It was also explained [13] that as the sintering temperature increases more amount of Co dissolves into the CGO lattice, leading to both less ionic and more p-type electronic carry in the grain bulk. The reason for decreasing ionic transport is the oxygen vacancy association with the small cobalt cations. In another investigation [15], Fe_2O_3 was added to CGO ($Ce_{0.8}Gd_{0.2}O_{1.9}$) as sintering aid in a composition of (1-x) $Ce_{0.8}Gd_{0.2}O_{1.9-x}$ (x) Fe_2O_3 where x ranged between (0.5and 1) mole. The powders were prepared by the milling method and processed conventionally. The investigators found that the addition of 0.5 atomic wt % Fe reduced the sintering temperature by ~ 200ºC, further increase in Fe content was not accompanied by any further decrease in sintering temperature, Fe-doping strongly promoted the densification rate of CGO ceramic bodies while undoped samples displayed only ~ 82 % density by sintering at 1300ºC (5 hrs.). Lima et al, [16], have studied the addition of copper oxide (CuO) on the crystal structure, densification and microstructure of Gd-doped ceria ($Ce_{0.9}Gd_{0.1}O_{2-\delta}$, CGO) synthesized by the polymeric precursor method. CuO content ranged between (0.5and 1) mole percent where the relative densities are set up to be 98 % for sintering temperature as low as 1000 ºC. The 1 mole % CuO on gadolinia doped ceria showed no detrimental influence on the total electrical conductivity.

The aim of the work is to research the role of co-doping and preparation conditions on the densification behavior of ceria ceramic bodies. This aim is realized through the use of rare earth oxides (Samaria and Yttria) and transition metal oxides (Fe) as co-dopants for cerium oxide and preparing the desired solid solution by the co-precipitation-hydrothermal techniques and studying the effect of these dopants on the properties of ceria- solid solution.

Experimental

Co-doped ceria powders were prepared by hydroxide co-precipitation of the corresponding cations accompanied by hydrothermal treatment under certain conditions using cerium nitrate hexahydrate ($Ce(NO_3)_3.6H_2O$, Strem, 99.99%), samarium nitrate hexahydrate ($Sm(NO_3)_3.6H_2O$, Aldrich, 99.9%), yttrium nitrate hexahydrate ($Y(NO_3)_3.6H_2O$, Aldrich, 99.9%), Fe metal, ammonia solution (NH_4OH) and absolute ethyl alcohol (C_2H_5OH). The amounts of cerium nitrate and the sources of the used dopants were dissolved in suitable amounts of de-ionized water. Fe metal was dissolved in small amount of concentrated nitric acid with gentle heating. The cerium oxide was co-doped with Fe oxide together with one of the rare earths (Sm or Y oxide). The corresponding amounts of the starting materials were calculated so as to fulfill the compositions mentioned in Table 1. Each dissolved mixture was co-precipitated by ammonia solution (NH_4OH). Ammonia solution was added drop wisely with continuous stirring till pH 10 was reached. The precipitated gels were transferred into Teflon–lined stainless steel autoclaves. Hydrothermally reaction was accomplished at 260ºC for 10 hours. For investigating the effect of autoclaving time, separate batches were autoclaved at the same temperature for different times 2, 5 and 15 hours. The autoclaves were cooled to room temperature

and the crystallized powder was washed several times with water followed by alcohol. The amount of the prepared powders were calcined at 600ºC for 2 hours, pressed uniaxially, and fired at different temperatures. As- prepared powders were inspected for their thermogravimetric behavior up to 1000ºC in ambient air using TGA 7 Perkin Elmer analyzer (USA) with a heating rate of 10º/ min. phase identification of the prepared powder was performed by XRD analysis using "Brucker D8" diffractometer (Advance, Germany) with monochromator CuKα radiation with Ni fitter and secondary monochromator at voltage 40 kV and current 40 mA. The average crystallite size, D, of the hydrothermally prepared powders was calculated from the Scherrer formula:

$D = \frac{0.9\lambda}{\beta \cos\theta}$ Where λ is the wavelength of CuKα radiation, θ is the diffraction angle.

β is the observed width at half height.

Infrared absorption spectra for the prepared powders were determined using a double beam Philips spectrograph (Nexus 670 FTIR spectrometer, Niederlands) in the frequency range of 4000-400 cm^{-1}. The Raman spectrum was determined for all the as- prepared powders using RFT-600 Raman spectrometer (Jasco, Italy) in the frequency range of 1000-20 cm^{-1} with a resolution of 8 cm^{-1}. The specific surface areas (S_{BET}) of the prepared powders were determined from the data on nitrogen adsorption isotherms at 77K using Java 2000 series, Quantachrome, USA. Before the measurements the fired samples were degassed at 200ºC under reduced pressure of 1.33x 10^{-3} Pa for 2hr. The obtained BET surface areas were ± 10 %. The morphology of the prepared powders was investigated using the transmission electron microscope (EM10-Zeiss, Germany).

The bulk density of the sintered bodies was determined by the mercury immersion method according to the following equation:

Bulk Density (g/cm^3) =

$$\frac{W_{air}(g) \times density_{(Hg)}(g/cm^3)}{W_{pan}(g) - W_{pan+disc}(g) + W_{air}(g)}$$

Where:

W_{air}: the weight of the disc in air, W_{pan}: the weight of the pan immersed in mercury,

$W_{pan+ disc}$: the weight of the disc and the pan immersed in mercury,

$Density_{(Hg)}$: density of mercury 13.6 (g/cm^3).

TABLE 1. Symbols of the single and co-doped CeO_2 investigated composition.

Symbol	Composition
10SDC	10 mol % Sm_2O_3: 90 mol % CeO_2
15SDC	15 mol % Sm_2O_3: 85 mol % CeO_2
20SDC	20 mol % Sm_2O_3: 80 mol % CeO_2
10YDC	10 mol % Y_2O_3: 90 mol % CeO_2
15YDC	15 mol % Y_2O_3: 85 mol % CeO_2
(20SDC)Fe	(20 mol % Sm_2O_3: 80 mol % CeO_2) 0.5 at. % Fe_2O_3
(10SDC)Fe	(10 mol % Sm_2O_3: 90 mol % CeO_2) 0.5 at. % Fe_2O_3
(15YDC)Fe	(15 mol % Y_2O_3: 85 mol % CeO_2) 0.5 at. % Fe_2O_3
(10YDC)Fe	(10 mol % Y_2O_3: 90 mol % CeO_2) 0.5 at. % Fe_2O_3

The relative densities of the different sintered ceria bodies were calculated according to the following equation:

Relative Density (%) = $\frac{BulkDensity(g/cm^3)}{TheoreticalDensity(g/cm^3)} \times 100$

Linear shrinkage is the decrease in the linear dimension of a sample when oven-dried, starting with a moisture content of the sample at the liquid limit. The linear shrinkage is measured as a percentage of the original length of the specimen as a function of sintering.

Percentage of linear shrinkage (%) =

$\frac{D_o - D_f}{D_o} \times 100$ Where: D_o is the original diameter of the sample (in mm), D_f is the diameter of the fired specimen (in mm)

The percentage of linear shrinkage was plotted against firing temperature of the different fired samples.

Results and Discussion

Characterization of (SDC) Fe and (YDC) Fe as-prepared co-doped powders

The TG and DTG curves of (20 mole % SDC) 0.5 wt. % Fe and (15 mole % YDC) 0.5 wt. % Fe are exhibited in Fig. 1 and 2. After the development of the low moisture content up to about 220ºC, a very limited amount of losses is recorded for both the Fe-doped solid solution powders up to 1000ºC due to the crystallization process and absorbed gases like CO_2. XRD patterns of (10, 15, and 20 mole % SDC) 0.5 wt. % Fe are seen in Fig. 3. it can be stated that the patterns are indexed to face-centered cubic structure of ceria (fcc). This result indicates that the existence of iron did not affect the formation of the solid solutions during the autoclaving process. In addition, there is a noticeable growth in crystallites with increasing Sm content in solid solutions. In Fig. 4 both the XRD patterns of SDC and (SDC) Fe powders are displayed together for comparison. It is clear from the strength of the X-ray peaks that the rate of increase in crystallinity in case of SDC powders is

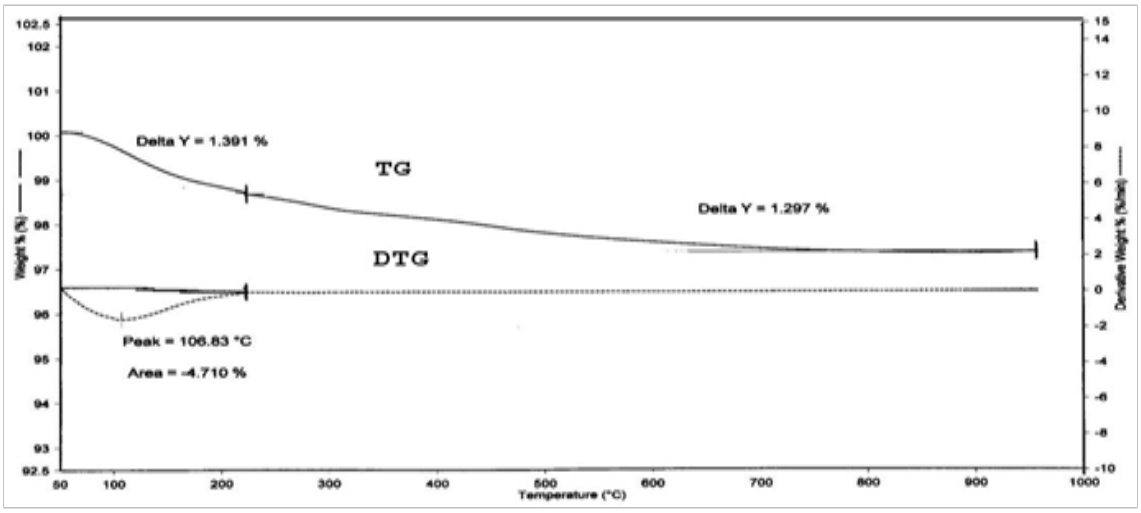

Fig. 1. Thermogravimetric of 20 mole% (SDC) Fe as-prepared powders up to 1000ºC.

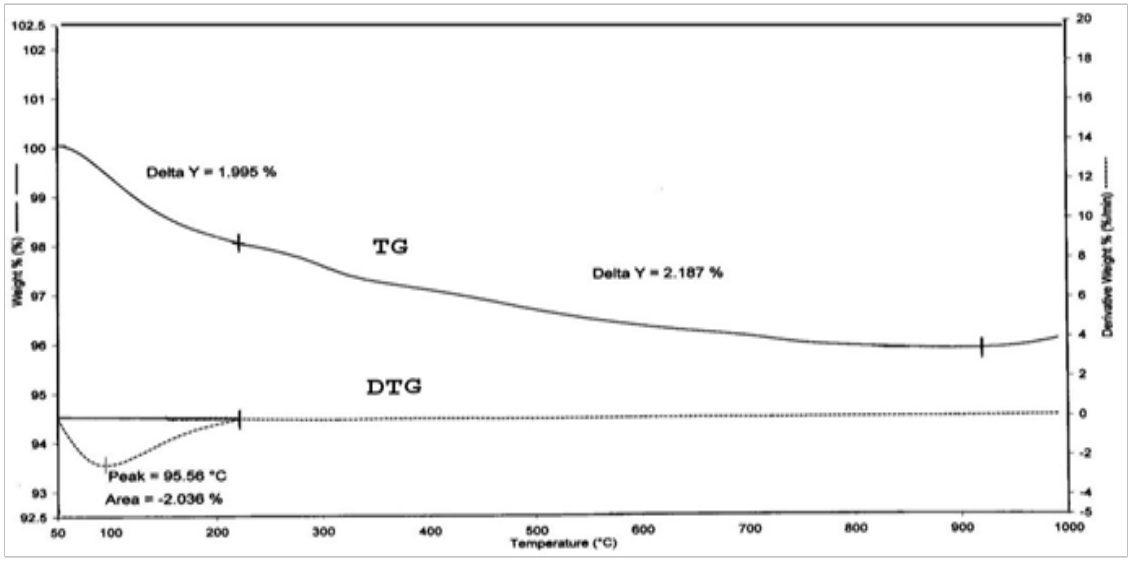

Fig. 2. Thermogravimetric of 20 mole% (YDC) Fe as-prepared powders up to 1000ºC.

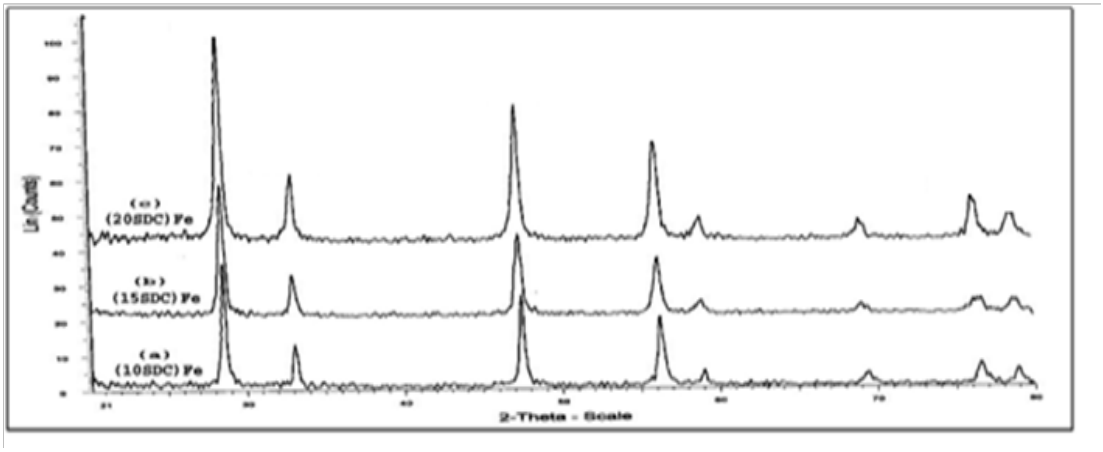

Fig. 3. XRD patterns of (SDC) Fe as-prepared powders.

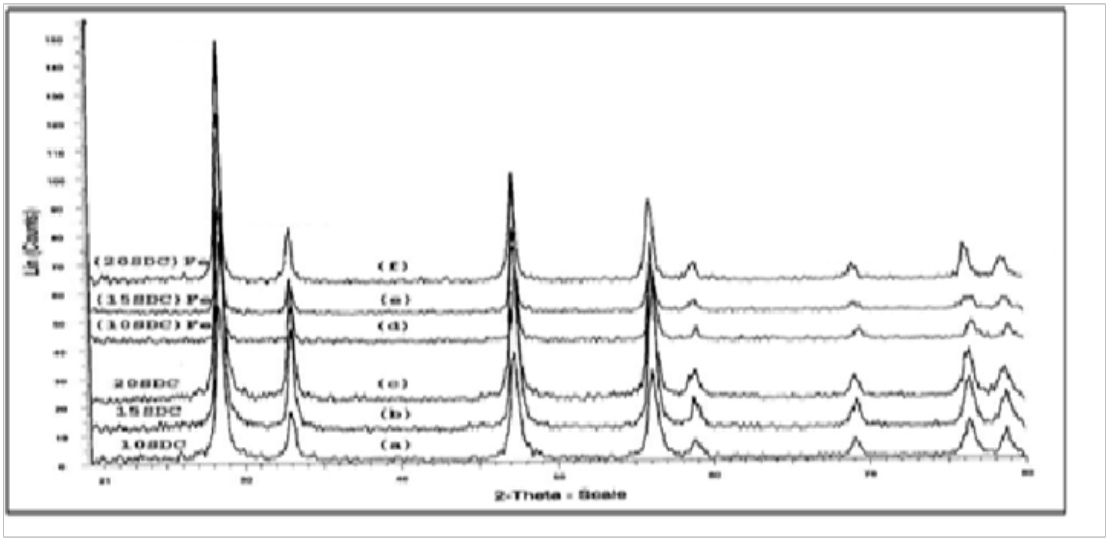

Fig. 4. Comparison between the XRD patterns of (SDC) and (SDC) Fe as- prepared powders.

TABLE 2. Crystallite sizes and specific surface areas of SDC and YDC

Sample Code	Crystallite Size (nm)	Specific Surface Area (m^2/g)
10SDC	17.5	76.31
15SDC	23.2	44.2
20SDC	22.5	46.4
10YDC	21.3	61.4
15YDC	22.5	58.7

TABLE 3. Crystallite sizes and specific surface areas of (SDC) Fe and (YDC) Fe.

Sample Code	Crystallite Size (nm)	Specific Surface Area (m^2/g)
(10SDC)Fe	10	52.0
(15SDC)Fe	11.7	40.7
(20SDC)Fe	15.1	27.7
(10YDC)Fe	7.2	42.0
(15YDC)Fe	8.8	39.5

greater than the rate for (SDC) Fe powders. This conclusion is confirmed by crystallite size values of the (SDC) Fe as-prepared powders, as calculated by Scherrer equation and given in Table 3. It is clear from the table that the samples containing Fe have crystallite sizes ranged between (10 and 15 nm) which is very smaller than those without iron addition (Table 2). It can be considered that the small Fe content (0.5 wt. %) played an important role in inhibiting the growth of crystallites during the hydrothermal oxidation process.

Similar observation was recorded by [17] in their work on Pr-doped ceria prepared by carbonate-coprecipitation process method in which they noticed that Pr-doping retards crystallite coarsening. However, they attributed this retardation to the variation in sizes between Pr^{3+} and Ce^{4+} cations which lead to local distortion in the crystal lattice. As is the case with (SDC) Fe solid solutions, the XRD peaks of the (YDC) Fe powders displayed in Fig. 5 showed that the iron addition is incorporated in the formed yttria-ceria solid solutions crystallized in the fcc fluorite structure (Cards No:75-0174 and 75-0175). The slight shift in X-ray peak positioning in YDC is also seen in the (YDC) Fe solid solutions. The XRD patterns of the YDC and (YDC) Fe in Fig. 6 shows an overall lowering in the peak intensities with the inclusion of iron in the crystal lattice of YDC. The crystallite sizes of the powders containing iron are around 7 and 8 nm which is much less than the original powders due to the growth inhibition effect of the Fe additions. The IR spectra of (SDC) Fe and (YDC) Fe are indicated in Fig. 7 and 8, respectively. The bands characteristic to ceria at about 850 and 1060 cm^{-1} are observed in the spectra jointly with the weak band at ~1380 cm^{-1} denoting the absorbed gases particularly CO_2. The slight shift in bands positioning from pure ceria is referred to the combination of different ions in its lattice. Figures 9 and 10 exhibit the TEM images of the as-prepared (SDC) Fe and (YDC) Fe powders. From the figures, we can see that the rounded-like nano-sized particles, sometimes separated and mostly agglomerated softly for most of these oxides. The soft agglomerates are rather observed as the rare earth dopants increase in content. The particle sizes ranges between (20 and 25 nm) which are less than the average sizes for the iron-free powders. The surface area values of the powders containing Fe addition (Table 3) are less than that for the Fe-free samples (Table 2) due to the inhibition effect of Fe addition. The surface area values decrease as the dopant content increases.

Raman spectra of (SDC) Fe and (YDC) Fe are exhibited in Fig. 11 and 12, respectively. It is clear from Fig. 11 that the band around 450 cm^{-1} denoting the T_{29} Raman active mode of the cubic fluorite solid solution [18 & 19] and decreases gradually in magnitude and intensity as the Sm content increases from 10 mole % to 20 mole %. Also, the weak band shoulder in the region of 580-650 cm^{-1}, denotes the existence of oxygen vacancies in the fluorite lattice [20] that weakened as the Sm content increases in the same order. Similarly, for the (YDC)Fe samples, the band around 450 cm^{-1} decreases in the intensity and the weak shoulder at 580-650 cm^{-1} is hardly seen (Fig. 12) as the (Y) content increases from 10 mole % to 15 mole %. Means that, the presence of Fe weakened the formation of the solid solution and oxygen vacancies as the Sm and Y contents are increased in the co-doped powders. It can be concluded from the data that the optimum solid solutions containing appropriate oxygen species in this group are obtained with (10SDC) Fe and (10YDC) Fe compositions. Figures 13 and 14 display the XRD peaks of (20SDC)Fe and (15YDC)Fe powders prepared by soaking at different times during the autoclaving process at 260ºC, respectively. The diffraction peaks get sharper with increased intensity as the soaking time increases from 5 to 15 hours indicating improved crystallinity. The results were acquired

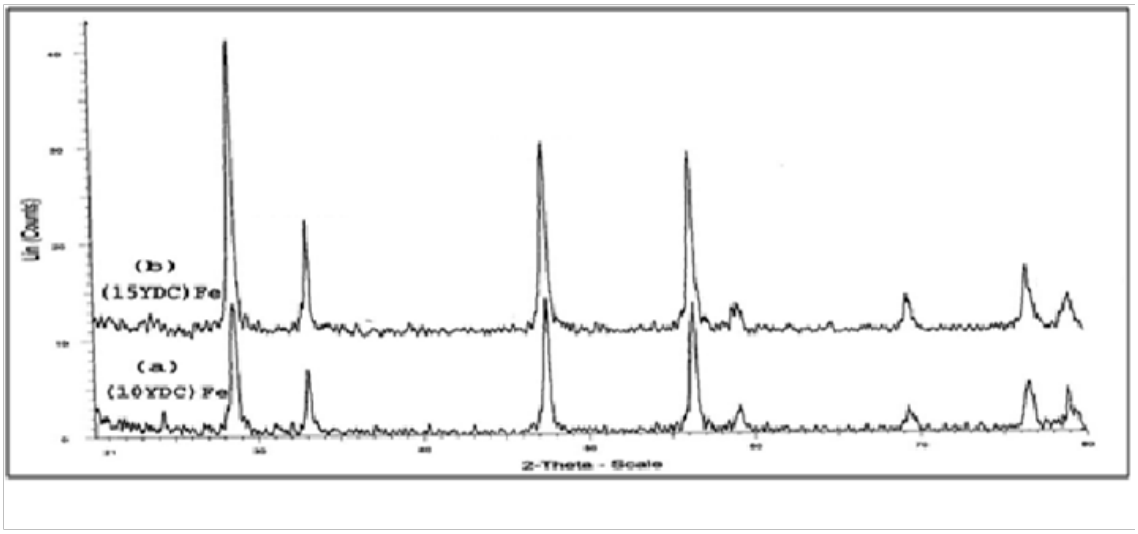

Fig. 5. XRD patterns of (YDC) Fe as- prepared prepared powders.

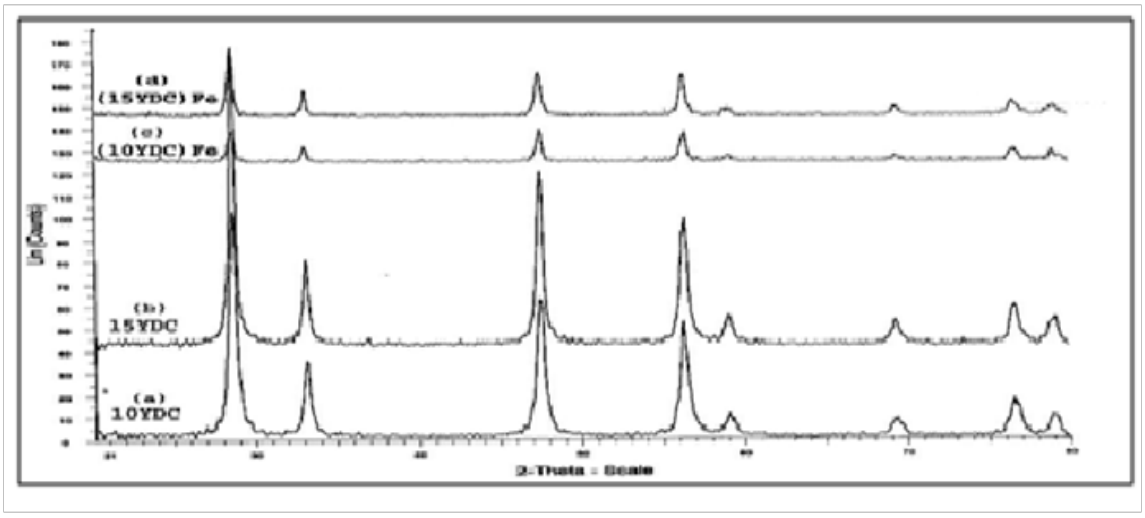

Fig. 6. Comparison between the XRD patterns of (YDC) and (YDC) Fe as- prepared powders.

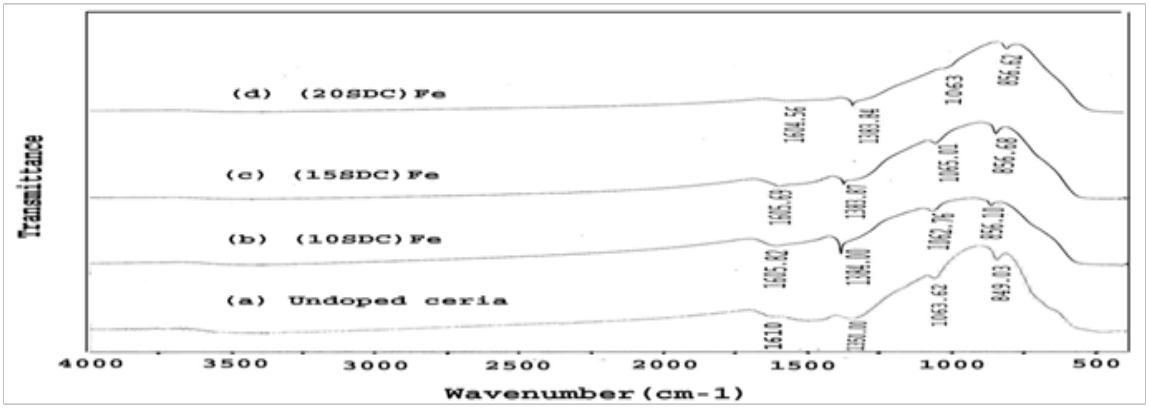

Fig. 7. Infrared spectra of un-doped and (SDC) Fe as- prepared powders.

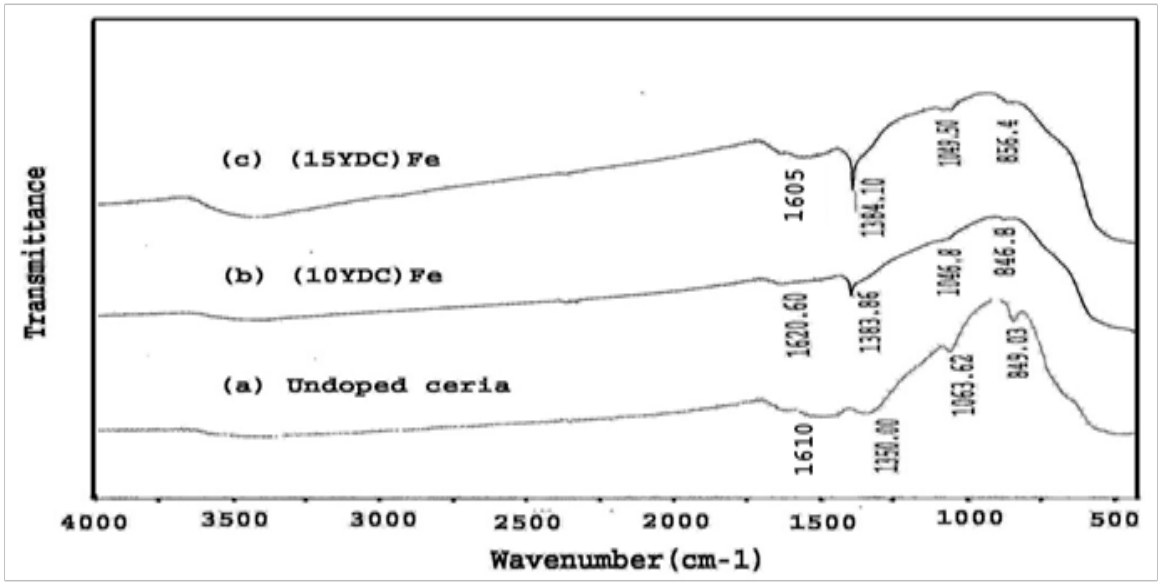

Fig. 8. Infrared spectra of un-doped and (YDC) Fe as-prepared powders.

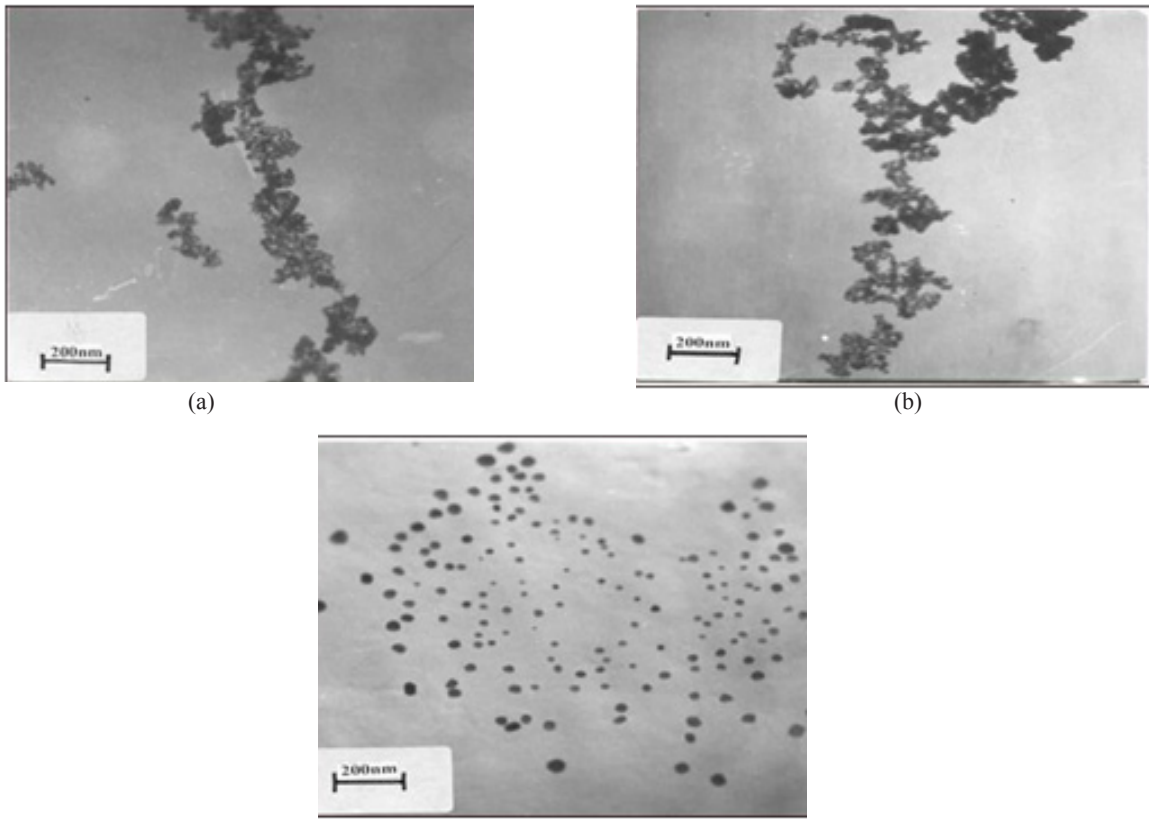

(a) (b)

(c)

Fig. 9. TEM of (a) (10SDC) Fe, (b) (15SDC) Fe and (c) (20SDC) Fe as- prepared powders.

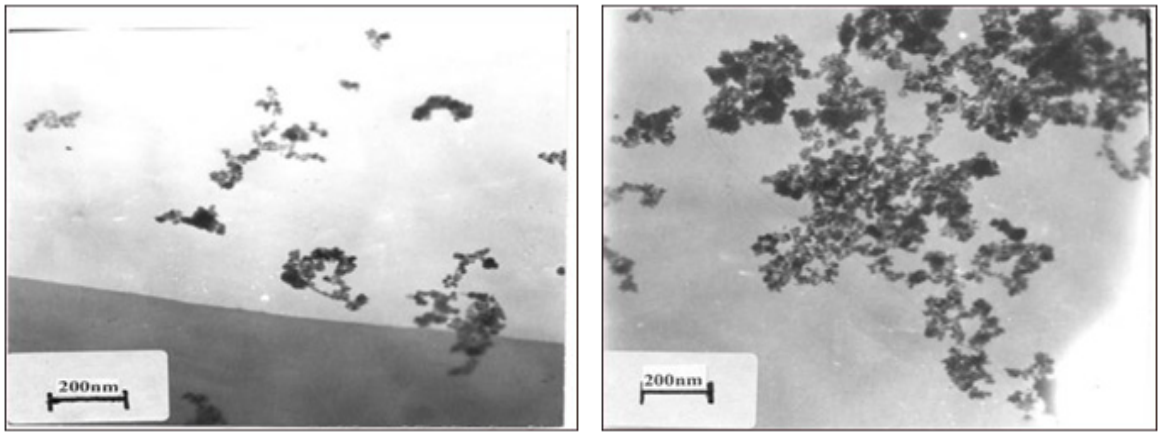

(a) (b)

Fig. 10.TEM of (a) (10YDC) Fe and (b) (15YDC) Fe as-prepared powders.

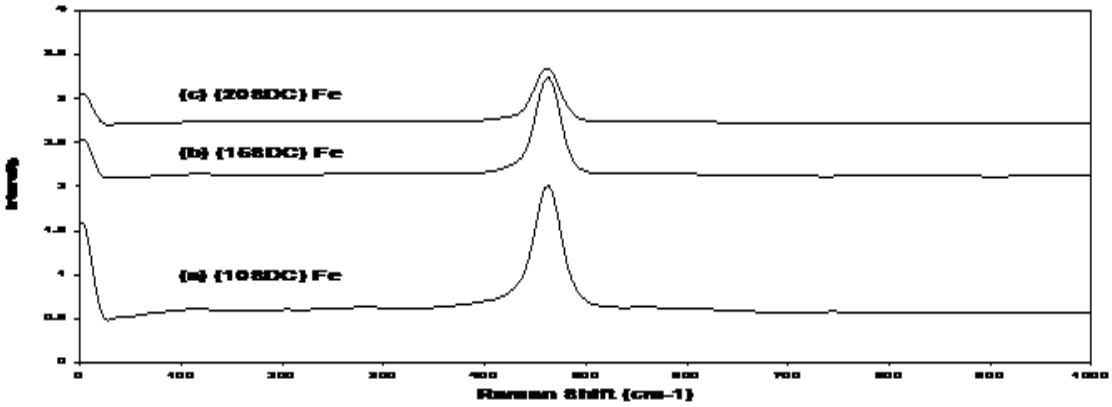

Fig. 11. Raman spectra of (SDC) Fe as-prepared samples.

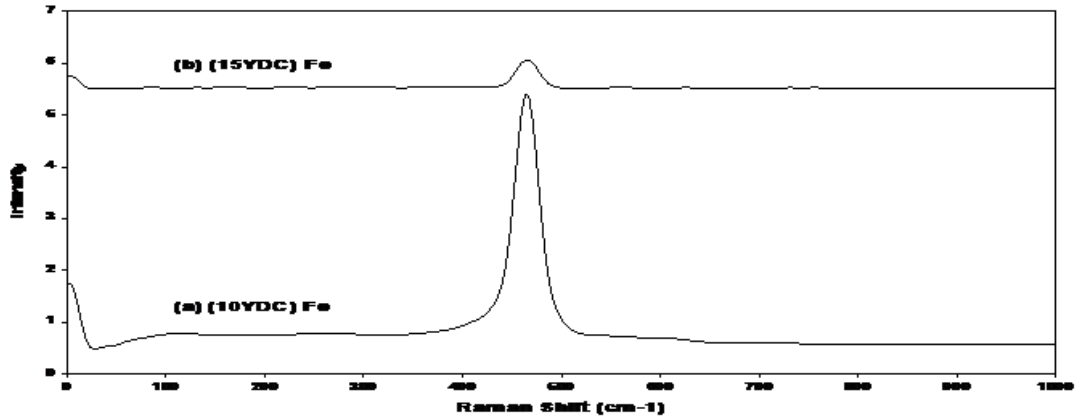

Fig. 12. Raman spectra of (YDC) Fe as-prepared samples.

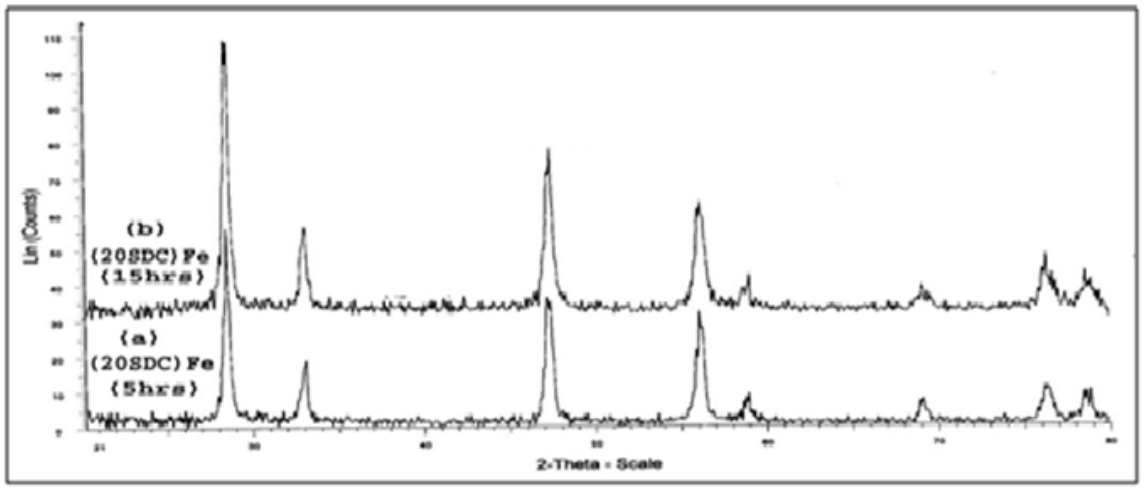

Fig. 13. Effect of autoclaving time on the crystallinity of (20SDC) Fe powders.

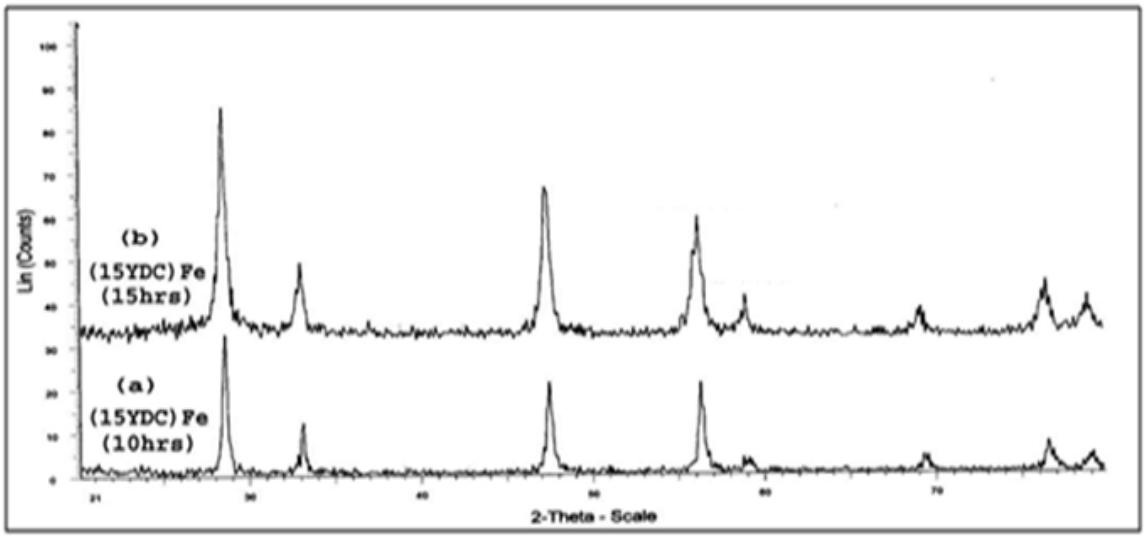

Fig. 14. Effect of autoclaving time on the crystallinity of (YDC) Fe powders.

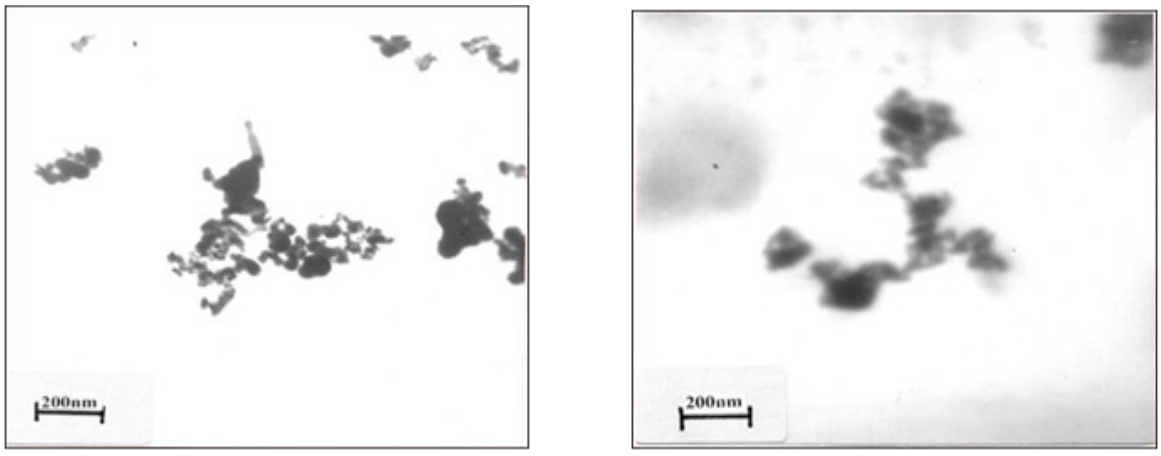

(a) **(b)**

Fig. 15. TEM photomicrographs of (20SDC) Fe autoclaved at (a) 2 hrs and (b) 15hrs.

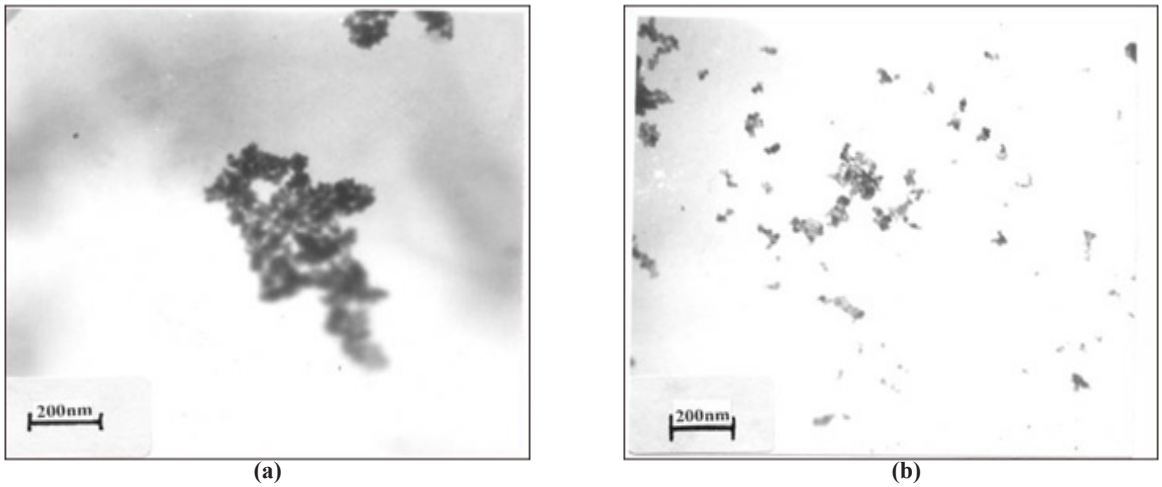

(a) (b)

Fig. 16. TEM photomicrographs of (15YDC) Fe autoclaved at (a) 2 hrs and (b) 15hrs.

TABLE 4. Crystallite sizes and specific surface areas of (20SDC) Fe and (15YDC) Fe at different autoclaving times.

Sample Code	Autoclaving Time (hrs)	Crystallite Size (nm)	Specific Surface Area (m^2/g)
(20SDC)Fe	5	14.1	28.0
	10	15.1	27.7
	15	20.6	24.3
(15YDC)Fe	10	7.2	42.0
	15	11.5	32.0

by Dikmen et al [21 & 22] they found that the ceria doped with La^{3+} and Gd^{3+} ions prepared by hydrothermal synthesis. The crystallite sizes of the prepared powders, calculated from the XRD data are seeing in Table 4. From the table it was observed that the crystallite size increased and the BET surface area values decreased as the autoclaving time increased from 5 to 15 hrs. The TEM photomicrographs of (20SDC) Fe and (15YDC) Fe powders are exhibited in Fig. 15 and 16, respectively. The semi-rounded nano-sized particles are observed with decreased tendency towards agglomeration as the autoclaving time is increased.

Densification of (SDC) Fe and (YDC) Fe powder compacts

The sintering curves of SDC and YDC powder compacts containing 0.5 wt. % Fe as a function of firing temperature are seen in Fig. 17 and 18, respectively. It is observed from the figures that a maximum relative density and maximum linear shrinkage for each composition (at 1200º or 1250ºC) is reached, after which a variable gradual decrease in both parameters is noticed on further firing up to 1350ºC. The maximum values of relative densities of (10SDC) Fe and of (10YDC) Fe are ~ 83 and 86.5 % of T.D. at 1200ºC, respectively. The maxima in relative densities of (20SDC) Fe and (15YDC) Fe are ~ 81.2 % and ~ 87 % of T.D., respectively by firing the powder at 1250ºC. The obtained results indicate that there is a shift towards lower temperatures of ~ 100º-150ºC in the maxima of densification, depending on the original composition of the solid solution, by the increase of 0.5 wt. % Fe to the SDC and YDC compositions. The linear shrinkage can also be seen from the figures. The results obtained prove that small addition of Fe_2O_3 lift the densification rates of both SDC and YDC powder compacts. Such sintering promotion of CeO_2 by small additions of Fe_2O_3 has been investigated

by many authors[9 & 23 & 24]. they obtained a 78 % relative density by sintering pure CeO_2 at 1430ºC, by the addition of 0.5 % Fe, relative density increased up to 87 % at lower temperature (1225ºC). They attributed the densification to a viscous flow mechanism. The rabid densification rate of Fe-doped sample at the lower temperature range increased the contact area of particles in the compacts, which promotes the diffusivity rate of matrix and thus enhances the densification during sintering. A prediction based on Herring's scaling laws [25], which states that the grain boundary diffusion increased by decreasing particle size. For the nano-sized powders and the relatively low sintering temperatures used in the present work, it seems plausible to suppose that grain boundary diffusion is one of the major controlling mechanisms for densification. The shift in sintering curves to low temperatures indicates that Fe addition promotes the rate of grain boundary diffusion. According to [24], in their work on influence of solid solution additives on sintering of ultrafine CeO_2 powders, dopants can influence the temple of the grain boundary by two main processes. First, the additive may shape a separate phase at the grain boundary by precipitation or by chemical reaction. The second phase can be formed as solid or liquid at the sintering temperature. In the second process, the cations may segregate in the grain boundary without the forming of a second phase, i.e. solute segregation effect.

In this work it is assumed that a reaction took place between the iron ions and the ions in the SDC and YDC solid solution major to the formation of a second phase, probably thin liquid phase, thus facilitating the movement of grain boundaries at the low temperature range so that a transmit in the densification maxima resulted. Similar reduction in sintering of 20 mole % Gd_2O_3-doped ceria was also reported by [26]. They attributed that behavior to the liquid-phase sintering happens in the Fe-doped ceria during sintering temperature. The above stated mechanisms, Chen and Chen [27 & 28] considered the influence of severely undersized dopant ions on the densification behavior of CeO_2 and similar oxides. The ionic size of Fe^{3+} (0.64 Å) is much smaller compared with that of matrix ion Ce^{4+} (0.97 Å) and those of Sm^{3+} (1.04) and Y^{3+} (0.93 Å). The incorporation of such undersized Fe^{3+} ion in the lattice of doped ceria could lead to certain asymmetry in lattice distortion leading to faster diffusivity of the matrix ion. X-ray diffraction patterns of (SDC) Fe and (YDC) Fe sintered bodies are shown in Fig. 19 and 20 respectively. The patterns do not show other lines except for the cubic fluorite structure of CeO_2. This result confirms that CeO_2 has a high solid solubility for many dopants. XRD patterns reflect also the crystallite growth due to sintering of the prepared powders. The sizes of crystallites the (SDC) Fe and (YDC) Fe sintered bodies, as calculated from X-ray data are given in Table 5. Despite the increase of

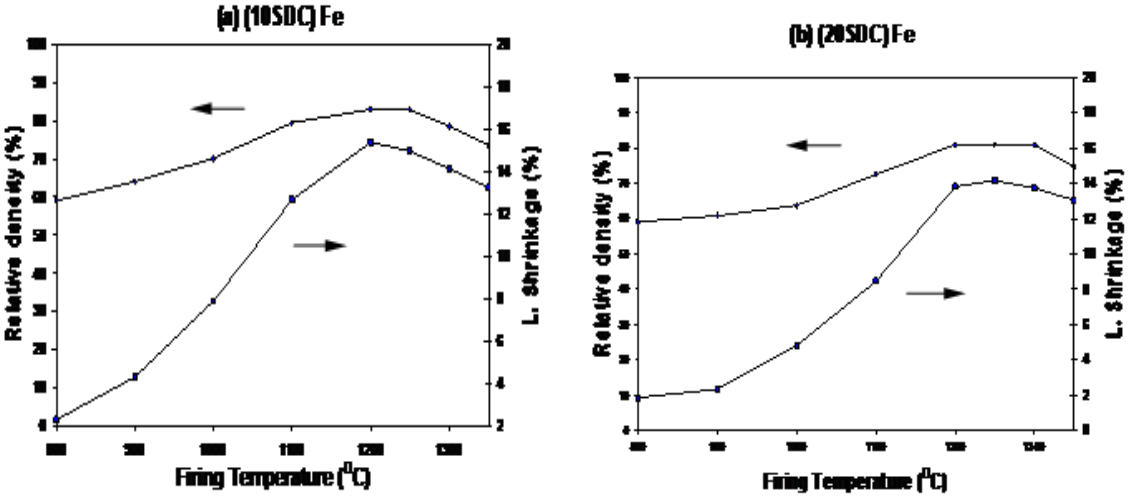

Fig. 17. Relative density (%) and linear shrinkage (%) of powder compacts: (a) (10 SDC) Fe and (b) (20 SDC) Fe at firing temperatures up to 1350°C.

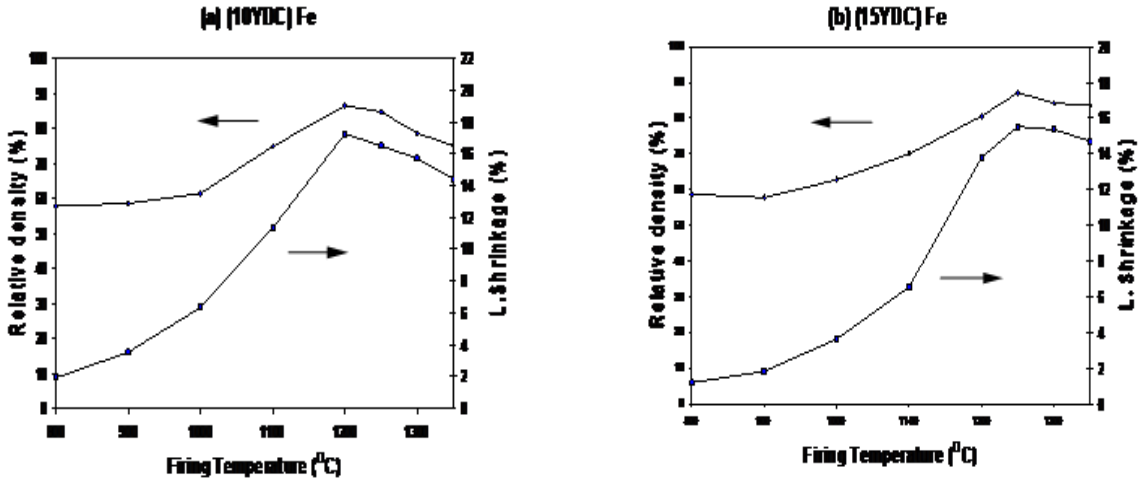

Fig. 18. Relative density (%) and linear shrinkage (%) of powder compacts: (a) (10YDC) Fe and (b) (15YDC) Fe at firing temperatures up to 1350°C.

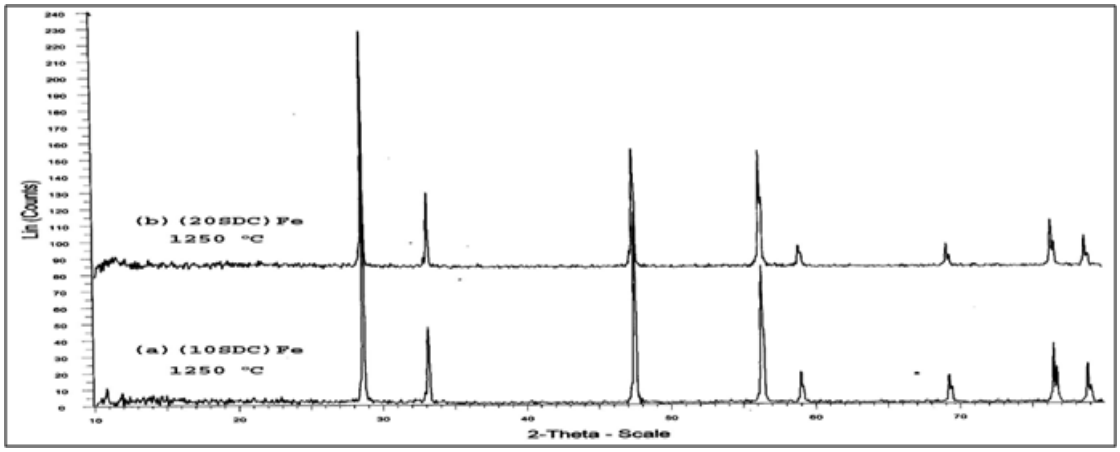

Fig. 19. XRD patterns of (Samaria-doped ceria) Fe sintered bodies.

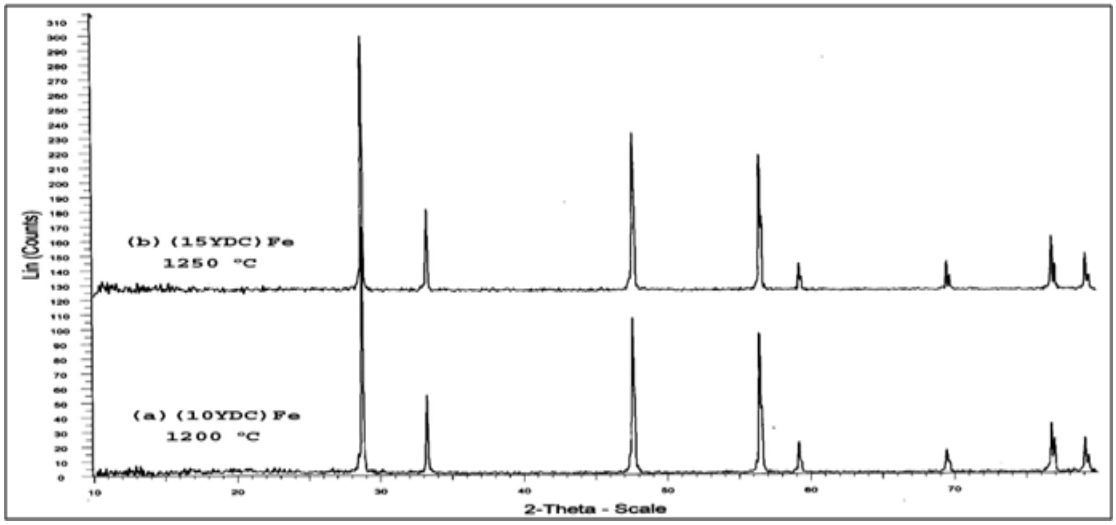

Fig. 20. XRD patterns of (Yttria-doped ceria) Fe sintered bodies.

crystallites, it is still possible to express the size values by nano units indicating the inhibition of excessive growth of crystallites due to the existence of dopants in the CeO_2 matrix. [24, 29 & 30].

Conclusions

- Sm-Fe and Y-Fe co-doped ceria solid solution were successfully prepared by hydrothermal method.
- The Fe co-doped powder samples, the appropriate fluorite-based solid solubility, high crystallinity and oxygen vacancy are achieved with the compositions (10SDC) Fe, (10YDC) Fe.
- The investigated compositions cold isostatic pressing is essential during forming of the compacts to bring the particle in close contact and overcome any agglomeration forces between particles, so that high densification.
- The incorporation of Fe in the SDC and YDC lattices led to faster rates of densification and lowering in the temperatures of maximum densification of the bodies.
- Iron addition of 0.5 wt. % lowered the $T_{max.}$ of densification by 100º-150ºC, so Fe is considered to be strong promoters for the sintering of ceria-based compositions.
- The Fe promoters to the SDC and YDC compositions changed the sintering mechanism of the bodies from diffusion controlled process into a viscous flow and the grain boundary mobility increased leading to faster densification.
- The deterioration of densification of the Fe co-doped bodies after the $T_{max.}$ is attributed to the too fast grain boundary migration and the possible increased liquid phase at the boundaries, leading to lots of pores trapped in grain boundaries cracks & bloating.
- The crystallite sizes of the maximum densified bodies for all the investigated compositions show noticeable increase resemble with the sizes of the corresponding as-prepared powders.

References

1. Steele BCH. Appraisal of $Ce_{1-y}Gd_yO_{2-y/2}$ electrolytes for IT-SOFC operation at 500°C, *Solid State Ionics,* **129**, 95–110 (2000).
2. Zheng Y, Wu L, Gu H, Gao L, Chen H, Guo L., The effect of Sr on the properties of Y-doped ceria electrolyte for IT-SOFCs, *J. Alloys Compd.,***486**, 586-589 (2009).
3. Blumenthal R. N. and Hofmaier R. L., The temperature and compositional dependence of the electrical conductivity of nonstoichiometric CeO_{2-x}, *J. Electrochem. Soc.,* **121**(1), 126-131 (1974).
4. Mahmoud Z.H., Novel Photosynthesis of CeO_2 nanoparticles from its salt with structural and spectral studyArticles in Press, Accepted Manuscript, *Egypt. J. Chem.,* Available Online from 12 September (2018), DOI: 10.21608/ejchem.2018.4013.1352.
5. Sh. M. El-Dafrawy, Mervat Farag, Sohier Abd El Hakam and Sh. M. Hassan, Structural and Catalytic Properties of Sulphated Zirconia doped by Zn Oxide, *Egypt. J. Chem*. **60** (2), 329- 345 (2017).
6. A. K. Aboul-Gheit, D. S. El-Desouki, S. M. Abdel-Hamid, S. A. Ghoneim, A. H. Ibrahim and F.K. Gad, Sulfated Zirconia Catalysts for Low Temperature Isomerization of n-Pentane, *Egypt. J. Chem.,* **55** (5), 509- 527 (2012).
7. S.A.M. Abdel-Hameed, N.A. Ghoniem and F. H. Margha, Development and Crystallization Study of Li2O-B2O3-SiO2 Glass Ceramic Rich with ZrO2, *Egypt. J. Chem.* **54**(1), 81- 97 (2011).
8. Gao Z, Liu X, Bergman B, Zhao Z. Enhanced ionic conductivity of $Ce_{0.8}Sm_{0.2}O_{2-\delta}$ by Sr addition, *J. Power Sources,* **208**, 225-231 (2012).
9. Zhang T., Hing P., Huang H. and Kilner J.; Densification, microstructure and Grain Growth in the CeO_2-Fe_2O_3 System (0≤ Fe ≤ 20 %), *J. Eur. Ceram. Soc.,* **21**, 2221-2228 (2001).
10. Babu A.S., Bauri R., Rare earth co-doped nanocrystalline ceria electrolytes for intermediate temperature solid oxide fuel cells (IT-SOFC), *ECS Transactions,* **57**, 1115–1123 (2013).
11. Babu A.S., Bauri R., Srinivas R. G., Processing and conduction behavior of nanocrystalline Gd-doped and rare earth co-doped ceria electrolytes, *Electrochimica Acta,* **209**, 541–550 (2016).

12. Fogg D. P., Abrantes J. C. C. and Perez-Coll D.; The Effect of Cobalt Oxide Sintering Aid on Electronic Transport in $Ce_{0.80}Gd_{0.20}O_{2-\delta}$ *Electrolyte, Electrochem. Acta,* **48**, 1023-1029 (2003).

13. Kovalevsky A. V., Kharton V. V. and Naumovich E. N.; Ionic and Electronic Conductivity of Ce (Gd, Co) $O_{2-\delta}$ Ceramics, *Inorg. Mat.,* **32**, 1230 (1996).

14. Zhang T. S., Ma J., Kong L. B., Chan S. H., Hing P. and Kilner J. A.; "Iron Oxide as an Effective Sintering Aid and A Grain Boundary Scavenger for Ceria-based Electrolytes", *Solid State Ionics,* **167**, 203-207 (2004).

15. Deraz N.M., Comparative Study on Synthesis and Characterization of Ceria Based Composite Oxides Containing Manganese Nano-Particles, *Egypt. J. Chem.* **53**(1), 61–76 (2010).

16. Limaa C.G.M., Santos T.H., Grilo J.P.F., Dutra R.P.S., Nascimento R. M., Rajesh S., Fonseca F.C., Macedo D.A., Synthesis and properties of CuO-doped $Ce_{0.9}Gd_{0.1}O_{2-\delta}$ electrolytes for SOFCs, *Ceramics International,* **41**, 4161–4168 (2015).

17. Wang Y., Mori T., Li J.-G. and Ikegami T.; Low-temperature Synthesis of Praseodymium-doped Ceria Nano-powders, *J. Am. Ceram. Soc.*, **85** (12), 3105-3107 (2002).

18. Ji Y., Liu J., He T., Wang J. and Su W.; The Effect of Pr Co-dopant on the Performance of Solid Fuel Cells with Sm-doped Ceria Electrolyte, *J. of Alloys and Compounds*, **389**, 317-322 (2005).

19. Godinho M. J., Goncdlves R. F., Santos L. P. S., Varela J. A., Longo E. and Leite E. R.; "Room Temperature Co-precipitation of Nano-crystalline CeO_2 and $Ce_{0.8}Gd_{0.2}O_{1.9-\delta}$ powder, *Mat. Let.* (2006), doi: 10.1016/ j. Mat. Let. 07.152 (2006).

20. Colon G., Pijolat M., Valivieso F. and Vidal H.; Surface and Structural Characterization of $Ce_x Zr_{1-x} O_2$ Mixed Oxides as Potential Three-way Catalyst Promoters, *J. Chem. Soc., Faraday Trans.,* **94**, 3717-3726 (1998).

21. Dikmen S., Shunk P., Greenblatt M. and Gocmez H., Hydrothermal Synthesis and Properties of $Ce_{1-x}Gd_xO_{2-\delta}$ *Solid Solutions, Solid State Sciences,* **4**, 585-590 (2002).

22. Dikmen S., Shuk P. and Greenblatt M., Hydrothermal Synthesis and Properties of $Ce_{1-x}La_xO_{2-\delta}$ *Solid Solutions, Solid State Ionics,* **126**, 89-95 (1999).

23. Zhang T. S., Ma J., Kong L. B., Zeng Z. Q., Hing P. and Kilner J. A., Final Stage Sintering Behaviour of Fe-doped CeO_2, *Mat. Sci. and Eng. B*, **103**, 177-183 (2003).

24. Rahman M. N. and Zhou Y. C.; Effect of Solid Solution Additives on the Sintering of Ultra-fine CeO_2 Powders, *J. Eur. Ceram. Soc.*, **15**, 939-950 (1995).

25. Herring C., Effect of Change of Scale on Sintering Phenomena, *J. Appl. Phys.*, **21**, 301-303 (1950).

26. Kleinlogel C. and Gauckler L. J., Sintering and Properties of Nanosized Ceria *Solid Solutions, Solid State Ionics,* **135**, 567-573 (2000).

27. Chen P. L., Chen I. W., Penner-Hahn J. E. and Tien T. Y., X-ray Absorption Studies of Ceria with Trivalent Dopants, *J. Am. Ceram. Soc.,* **74**, 958-967 (1991).

28. Chen P. L., Chen I. W., Pennar-Hahn J. E., Effect of Dopants on Zirconia Stabilization—An X-ray Absorption Study: III, Charge-Compensating Dopants, *J. Am. Ceram. Soc.,* **77**, 1289-1295 (1994).

29. Distine R. T., Blumenthat R. N. and Kuech T. F., Ionic Conductivity of Calcia, Yttria and Rare Earth-doped Cerium Oxide, *J. Electrochem. Soc.,* **126** (2), 264-269 (1979).

30. Yahiro H., Eguchi Y., Eguchi K. and Arai H., Oxygen Ion Conductivity of the Ceria-samarium Oxide System with Fluorite Structure, *J. Appl. Electrochem.,* **18**, 527-531 (1988).

توصيف متوالفات السيريا المشابه بالسماريا اوالايتريا ومزدوجة الاشابه بعنصر الحديد والمحضره بطريقة الترسيب المزدوج- المعالجه الحراريه

هيام عبدالعزيز بدر، نبيل محمد غنيم، احمد المغربى
قسم السيراميك - المركز القومى للبحوث - ١٢٦٢٢- - الدقى - القاهره - مصر.

مساحيق السيريا المشابه بالسماريا والايتريا تم تحضيرها بطريقة الترسيب المزدوج- المعالجه الحراريه وتم اضافة عنصر الحديد بنسبه ثابته لجميع المتوافات وهى 0.5 % . وقد تم توصيف المساحيق الناتجه باستخدام التحليل الحرارى الوزنى وانحراف الأشعه السينيه وأطياف الأشعه تحت الحمراء والميكروسكوب الإلكترونى النافذ وأيضًا تحليل طيف رامان. وتم دراسة تأثير وقت المعالجه الحراريه على الحجم البللورى. وقد تم كبس المساحيق المحضره ثم تلبيدها عند درجات حراره مختلفه . وتم التحقق من الكثافه ومعدل الانكماش للاجسام الملبده. واظهرت نتائج انحراف الأشعه السينيه ان المساحيق تتبلورفى الحجم البللورى المكعب مع تحسن فى التبلور. وجود الحديد فى المتوالفات يقلل من درجة التبلور. وقد أوضحت صور الميكروسكوب الإلكترونى النافذ أن المساحيق مزدوجه الاشابه متجانسه دقيقه فى أحجامها وشبه كروية الشكل وتوزيع حجمى ضيق. وتم التوصل الى ان افضل المتوالفات هى عينات السيريا المشابه بعشره فى المائه سماريا ومزدوجة الاشابه بالحديد Fe(10SDC) والسيريا المشابه بعشره فى المائه ايتريا ومزدوجة الاشابه بالحديد Fe (10YDC).